43rd AIAA Aerospace Sciences Meeting and Exhibit, 10-13 January 2005, Reno, Nevada

Highly Accurate Numerical Simulations of Pulsating One-Dimensional Detonations

Andrew K. Henrick*
University of Notre Dame, Notre Dame, Indiana, 46556-5637, USA

Tariq D. Aslam†
Los Alamos National Laboratory, Los Alamos, New Mexico, 87545, USA

Joseph M. Powers‡
University of Notre Dame, Notre Dame, Indiana, 46556-5637, USA

A novel, highly accurate numerical scheme based on shock-fitting coupled with high order spatial and temporal discretization is applied to a classical unsteady detonation problem to generate solutions with unprecedented accuracy. The one-dimensional reactive Euler equations for a calorically perfect mixture of ideal gases whose reaction is described by single-step irreversible Arrhenius kinetics are solved in a series of calculations in which the activation energy is varied. In contrast with nearly all known simulations of this problem, which converge at a rate no greater than first order as the spatial and temporal grid is refined, the present method is shown to converge at a rate consistent with the fifth order accuracy of the spatial discretization scheme. This high accuracy enables more precise verification of known results and prediction of heretofore unknown phenomena. To five significant figures, the scheme faithfully recovers the stability boundary, growth rates, and wave-numbers predicted by an independent linear stability theory in the stable and weakly unstable regime. As the activation energy is increased, a series of period-doubling events are predicted, and the system undergoes a transition to chaos. Consistent with general theories of non-linear dynamics, the bifurcation points are seen to converge at a rate for which the Feigenbaum constant is 4.66 ± 0.09, in close agreement with the true value of $4.669201\ldots$. As activation energy is increased further, domains are identified in which the system undergoes a transition from a chaotic state back to one whose limit cycles are characterized by a small number of non-linear oscillatory modes. This result is consistent with behavior of other non-linear dynamical systems, but not typically considered in detonation dynamics.

I. Introduction

Improvements in the accuracy of prediction of physical phenomena are enabled by advances in both computational hardware and software. Computational science and engineering has made rapid progress over the past decades to the point where simulation of physically motivated problems which once required the significant resources of a super-computer can now be solved on an inexpensive personal computer. Certainly, some of this expanded capability is attributable to improvements in computational hardware. The celebrated Moore's Law,[1] an empirical observation which originally held that the number of transistors per integrated circuit doubles roughly every year, is a popular embodiment of this notion. Variants apply to other aspects of hardware such as hard disk and random-access-memory (RAM) storage capacity, and parallel architecture design. Less celebrated, but perhaps even more important as physical limitations dampen the

*Ph.D. Candidate, ahenrick@nd.edu.
†Detonation Physics Team, aslam@lanl.gov.
‡Associate Professor, AIAA Associate Fellow, powers@nd.edu.

rate of advancements in hardware,[2] are simultaneous advances in computational algorithms. In contrast to hardware, which the computational mechanician generally treats as a commodity, advances in algorithm development are in need of the skills of the artisan; for specialized problems, there are often precise tools which can be employed with a realization of remarkable gains. Improved algorithms enable the more rapid solution of problems relative to existing methods when the same computational resources are employed; moreover, the solution of heretofore unsolvable problems is often admitted.

In this paper, we describe and implement a new algorithm tailored to simulate a well-established model problem: one-dimensional unsteady detonation. The new predictions are *many orders of magnitude more precise* than those previously published; this enhanced precision enables the prediction of remarkable new bifurcation phenomena. The model on which we focus simulates the key mechanisms of convection and single step exothermic reaction. For tractability, simpler constitutive relations than those which are appropriate for real materials are employed, and all diffusive transport neglected. Consequently, direct comparison with experimental results will be impossible. However, the techniques described here can, in principle, be adapted to models which better represent actual physical systems with detailed kinetics and complex state equations.[3] Nevertheless, the widely disparate length scales present in such systems pose such a formidable modeling challenge that it is unlikely that a fully resolved unsteady detonation for a system with detailed kinetics exists as of yet.[4]

In particular, this study presents numerical predictions of classical pulsating one-dimensional detonations propagating in an inviscid reacting calorically perfect ideal gas whose chemistry is modeled by one-step irreversible kinetics. The numerical solutions formally converge at a fifth order rate so that high accuracy is achieved at a moderate computational cost. The high rate of convergence is obtained using a shock-fitting scheme in which the reactive Euler equations are transformed to a shock-attached frame. A method of lines approach is used to discretize the resulting partial differential equations (PDEs) on a uniform spatial grid.[5] In continuous regions of the flow, spatial gradients are modeled by a fifth order mapped weighted essentially non-oscillatory scheme (WENO5M).[6] The resulting ordinary differential equations in time are then solved by a fifth order Runge-Kutta technique.[7] While the method chosen is specific and requires a discretization of the conservative form of the governing equations, we speculate that comparable accuracy could be achieved with any numerically stable fifth order discretization of conservative or non-conservative forms of the equations, provided that discretization is consistently coupled with a shock-fitting scheme of the same order.

Unsteady detonations predicted by the model employed here have been widely studied for over forty years. A partial list[8−20] summarizes some of the many approaches: linear stability via normal modes analysis, asymptotic techniques, method of characteristics, and direct numerical simulation using shock-capturing, shock-tracking and/or adaptive mesh refinement techniques. Linear stability analysis gives the most rigorous results, but cannot capture the non-linear dynamics or long-time limit cycle behavior. The method of characteristics, when coupled with a high order method for solution of ordinary differential equations, can give accurate results, at the expense of algorithmic complexity and difficulty in accommodating flows with multiple discontinuities. Shock capturing techniques are easy to implement, but results are corrupted by order one errors at the shock which propagate into the entire flow field, rendering it difficult to precisely identify fine scale dynamics.[21−24] Methods which do have high order accuracy for continuous solutions, when coupled with a shock-capturing scheme, always reduce that accuracy to at most first order. Although shock-tracking[9,11,12,18] and shock-fitting schemes[19] can in principle eliminate the order one errors at the shock, high rates of global convergence have not been demonstrated to date.

The true high order accuracy of the new numerical algorithm is the principal novelty of this work; less accurate versions of most results have appeared previously in the literature. We compare our results to two of the best of recent studies: Kasimov and Stewart[19] and Ng, *et al.*[20] Several test problems are exploited to verify the accuracy of the scheme. In particular, for unstable detonations it becomes possible to predict, with high precision and moderate resolution, both the growth rates and frequencies of the same unstable modes which have been independently predicted by linear stability analysis. The results are then extended into the non-linear regime to predict the ultimate limit cycle behavior. Relative to recent related calculations,[19,20] those presented here are resolved in roughly two orders of magnitude more detail, which allows a clearer elucidation of the structurally rich bifurcation phenomena. In particular, new windows of parameter space are identified in which low frequency behavior is predicted in an otherwise chaotic region.

The plan of the paper is as follows. First, the governing equations and associated jump conditions are specified. An evolution equation for the shock state is derived, which is commonly referred to as the shock-change equation.[25] A description of the fifth order scheme is then presented. The solution to various test

problems is given. These include comparisons with the stable Zel'dovich-von Neumann-Döring (ZND) solution, growth rate and frequency of linearly unstable ZND waves, and fully time-dependent and non-linear detonation pulsation flows. A detailed bifurcation diagram shows how the long-time limit of the detonation wave speed behaves as activation energy is varied. Period-doubling bifurcations, identified earlier,[15,20] are found to much greater precision, and several new modes of behavior are given. It is also confirmed that the convergence of the period-doubling bifurcation points is in agreement with the general theory of Feigenbaum.[26,27]

II. Governing Equations

The one-dimensional unsteady reactive Euler equations for a calorically perfect ideal gas which undergoes a single irreversible reaction are expressed in conservative form as

$$\frac{\partial \rho}{\partial t} + \frac{\partial}{\partial \xi}(\rho u) = 0, \tag{1}$$

$$\frac{\partial}{\partial t}(\rho u) + \frac{\partial}{\partial \xi}\left(\rho u^2 + p\right) = 0, \tag{2}$$

$$\frac{\partial}{\partial t}\left(\rho\left(e + \frac{1}{2}u^2\right)\right) + \frac{\partial}{\partial \xi}\left(\rho u\left(e + \frac{1}{2}u^2 + \frac{p}{\rho}\right)\right) = 0, \tag{3}$$

$$\frac{\partial}{\partial t}(\rho\lambda) + \frac{\partial}{\partial \xi}(\rho u\lambda) = k\rho(1-\lambda)\exp\left(-\frac{\rho E}{p}\right), \tag{4}$$

$$e = \frac{1}{\gamma - 1}\frac{p}{\rho} - \lambda q. \tag{5}$$

Here, the ordinary laboratory frame Cartesian distance coordinate is ξ, while time is t. Dependent variables in Eqs. (1-5) are density ρ, particle velocity u, pressure p, specific internal energy e and reaction progress λ. Parameters are reaction kinetic rate constant k, activation energy E, ratio of specific heats γ, and heat release per unit mass q. Equations (1-5) are expressions of, respectively, the conservation of mass, ξ-momentum, and energy, evolution of species, and a caloric state relation. Equation (4) models the irreversible reaction $A \rightarrow B$ in which species A and B have identical molecular masses and specific heats. The mass fractions of each species, Y_A and Y_B, are given in terms of the reaction progress variable by the relations $Y_A = 1 - \lambda$ and $Y_B = \lambda$.

Equations (1-5) are supplemented by the following standard Rankine-Hugoniot conditions at the shock jump:

$$\rho_s(D(t) - u_s) = \rho_o(D(t) - u_o), \tag{6}$$

$$p_s - p_o = (\rho_o(D(t) - u_o))^2\left(\frac{1}{\rho_o} - \frac{1}{\rho_s}\right), \tag{7}$$

$$e_s - e_o = \frac{1}{2}(p_s + p_o)\left(\frac{1}{\rho_o} - \frac{1}{\rho_s}\right), \tag{8}$$

$$\lambda_s = \lambda_o. \tag{9}$$

Here, D is the shock velocity, which in general is time-dependent; the subscript s denotes the shock state, and the subscript o denotes the ambient state. Note that the shock states in Eqs. (6-9) can be determined in terms of the ambient state and the shock velocity. It is assumed that no reaction takes place upstream of the shock; *i.e.* the source term in Eq. (4) is activated only for fluid particles which have passed through the shock.

For the shock-fitting numerical scheme, Eqs. (1-4) are transformed to a frame that is fixed to the shock front. To this end, a new spatial variable is taken to be

$$x = \xi - \int_0^t D(\tau)d\tau, \tag{10}$$

where the shock is initially presumed to be at $\xi = 0$, and thus for all time the shock locus is $x = 0$. Here τ is a dummy variable. Under this transformation, one recovers the following conservation laws:

$$\frac{\partial \rho}{\partial t} + \frac{\partial}{\partial x}(\rho(u - D)) = 0, \tag{11}$$

$$\frac{\partial}{\partial t}(\rho u) + \frac{\partial}{\partial x}(\rho u(u-D)+p) = 0, \tag{12}$$

$$\frac{\partial}{\partial t}\left(\rho\left(e+\frac{1}{2}u^2\right)\right) + \frac{\partial}{\partial x}\left((u-D)\rho\left(e+\frac{1}{2}u^2\right)+up\right) = 0, \tag{13}$$

$$\frac{\partial}{\partial t}(\rho\lambda) + \frac{\partial}{\partial x}(\rho(u-D)\lambda) = k\rho(1-\lambda)\exp\left(-\frac{\rho E}{p}\right). \tag{14}$$

The particle velocity, u, is still measured in the laboratory frame. To this point, there is nothing different than earlier shock-fitting formulations.[19] The only critical issue in solving Eqs. (11-14) is that the shock velocity, D, and shock relations, Eqs. (6-9), need to be directly incorporated into the solution. At the shock, in particular, one needs to apply the exact shock relations in a consistent manner with the evolution PDEs. At the shock, all state variables are functions of the quiescent state and the shock velocity; they are not independent of one another. A simple way to account for this is to derive an evolution equation at the shock based on the PDEs and the shock relations. This procedure results in what is often referred to as the shock-change equation.[25]

A. Shock-Change Equation

The shock-change equation describes the evolution of the shock velocity as a function of time. This relationship can take on various forms which are mathematically equivalent. A new and particularly useful form is derived here. First, assuming $\lambda_o = 0$, one determines the momentum at the shock state from Eqs. (5-9) to be

$$\rho_s u_s = \frac{\rho_o(D-u_o)\left(\gamma(\rho_o(D-u_o)u_o - 2p_o) + \rho_o(2D^2 - 3Du_o + u_o^2)\right)}{\gamma(2p_o + \rho_o(D-u_o)^2) - \rho_o(D-u_o)^2}. \tag{15}$$

As Eq. (15) is a function of D alone, one has

$$\frac{dD}{dt} = \left(\frac{d}{dD}(\rho_s u_s)\right)^{-1}\frac{d}{dt}(\rho_s u_s), \tag{16}$$

from the chain rule. Next, the total derivative following the shock in the shock-fitted coordinate is given by

$$\left.\frac{d}{dt}\right|_{x=0} = \left.\frac{\partial}{\partial t}\right|_{x=0} + \underbrace{\left.\frac{dx}{dt}\right|_{x=0}}_{=0}\left.\frac{\partial}{\partial x}\right|_{x=0} = \left.\frac{\partial}{\partial t}\right|_{x=0}, \tag{17}$$

since the velocity of the shock in the fitted coordinate system is zero. Thus, Eq. (12) becomes

$$\left.\frac{d(\rho_s u_s)}{dt}\right|_{x=0} + \frac{\partial}{\partial x}(\rho u(u-D)+p)|_{x=0} = 0, \tag{18}$$

at the shock. Lastly, substituting Eq. (18) into Eq. (16) yields the shock-change equation

$$\frac{dD}{dt} = -\left(\frac{d(\rho_s u_s)}{dD}\right)^{-1}\left.\left(\frac{\partial}{\partial x}(\rho u(u-D)+p)\right)\right|_{x=0}. \tag{19}$$

Equation (19) relates the shock acceleration to the momentum flux gradient at the shock. Other, mathematically equivalent forms of the shock-change equation could have been used, but there are two reasons this particular form was chosen. Firstly, the momentum flux gradient is something that will already be computed elsewhere in the flow. More importantly, it scales easily with shock velocity, so that the first term on the right hand side of Eq. (19) is well behaved in both the weak and strong shock limits. That is not the case for mass or energy equations. Other combinations of the equations may be well behaved as well, but this is adequate for what follows in the next section.

III. Numerical Method

Here, the details of the high order shock-fitting numerical algorithm are presented. A point-wise method of lines approach[5] is used. This method simplifies the required coding, allows separate temporal and spatial discretizations, and also allows for the incorporation of source terms. In the following sections, the computational grid will be defined, the WENO5M spatial discretization scheme[6] will be outlined, and the temporally fifth order Runge-Kutta scheme for time discretization[7] will be given.

A. Grid

Written in vector notation, Eqs. (11-14) take on the form

$$\frac{\partial}{\partial t}\mathbf{u} + \frac{\partial}{\partial x}\mathbf{f}\left(\mathbf{u}\right) = \mathbf{s}\left(\mathbf{u}\right). \tag{20}$$

Here the vector $\mathbf{u}$ is used to denote the set of conserved dependent variables,

$$\mathbf{u} = \left(\rho, \rho u, \rho\left(e + \frac{1}{2}u^2\right), \rho\lambda\right)^T. \tag{21}$$

Strictly speaking, $\rho\lambda$ is not conserved, but evolves due to the reaction source term. It is traditional to label it a conserved variable as well, as it is the proper divergence formulation of the reaction kinetics model. The vector $\mathbf{f}$ is a set of fluxes of each conserved quantity, and $\mathbf{s}$ is a source. A uniform Cartesian grid is used to discretize the domain $x \in [x_{min}, x_{max}]$, with $N_x + 1$ equally spaced nodes, $x_{min} < 0$, and $x_{max} = 0$. Next, one allows the semi-discretization $\mathbf{u}(x,t) \rightarrow \mathbf{u}_i(t)$ and the full discretization $\mathbf{u}_i(t) \rightarrow \mathbf{u}_i^n$, where the semi-discretized and fully discretized numerical solution vectors are denoted by $\mathbf{u}_i$ and $\mathbf{u}_i^n$, respectively. Here, i is the spatial node number corresponding to the location $x_i = x_{min} + i\Delta x$, where $\Delta x = -x_{min}/N_x$, and n is the time level corresponding to $t_n = \sum_{m=1}^{n} \Delta t_m$, where Δt_m is the time step for each integration step.

B. Spatial Discretization

Following spatial discretization, Eq. (20) can be approximated as a system of ordinary differential equations in t:

$$\frac{d\mathbf{u}_i}{dt} = \mathbf{L}\left(\mathbf{u}_i\right), \tag{22}$$

where the operator $\mathbf{L}$ is a discrete approximation to the continuous convection and source operators of Eq. (20):

$$\mathbf{L}\left(\mathbf{u}_i\right) \approx \left(-\frac{\partial}{\partial x}\mathbf{f}\left(\mathbf{u}\right) + \mathbf{s}\left(\mathbf{u}\right)\right)\Big|_{x=x_i}. \tag{23}$$

Next, the definition of $\mathbf{L}$ for various spatial nodes are defined.

1. *Nodes $i < 0$*

For nodes for which $i < 0$, which are necessary for calculation of some fluxes, a zero gradient condition is enforced. Formally, this introduces spurious waves at the boundary. However, as a check, the forward characteristic emanating from this boundary was calculated, and it was guaranteed that the domain was sufficiently large so as to prevent corruption of the shock and reaction zone structure from this downstream acoustic noise.

2. *Nodes $0 \leq i \leq N_x - 3$*

Next, general nodes at least four nodes removed from the shock are considered. For $\mathbf{L}(\mathbf{u}_i)$ the WENO5M scheme[6] with a local Lax-Friedrichs solver is used. This scheme is a conservative flux difference method, which has been shown to be stable, and yields the proper viscosity-vanishing solution to Eqs. (1-4). The operator $\mathbf{L}(\mathbf{u}_i)$ is given by:

$$\mathbf{L}(\mathbf{u}_i) = -\frac{\hat{\mathbf{f}}_{i+1/2} - \hat{\mathbf{f}}_{i-1/2}}{\Delta x} + \mathbf{s}\left(\mathbf{u}_i\right), \tag{24}$$

where $\hat{\mathbf{f}}_{i+1/2}$ and $\hat{\mathbf{f}}_{i-1/2}$ are numerical approximations to the flux function, $\mathbf{f}(\mathbf{u})$, and $\mathbf{s}\left(\mathbf{u}_i\right)$ is a simple evaluation of the source terms at node x_i.

In particular, for the local Lax-Friedrichs scheme, one takes

$$\hat{\mathbf{f}}_{i+1/2} = \hat{\mathbf{f}}^{+}_{i+1/2} + \hat{\mathbf{f}}^{-}_{i+1/2} \tag{25}$$

where for each component, $\hat{f}^{\pm}$, of the vector $\hat{\mathbf{f}}^{\pm}$ one has

$$\hat{f}^{+}_{i+1/2} = \Xi(f^{+}_{i-2}, f^{+}_{i-1}, f^{+}_{i}, f^{+}_{i+1}, f^{+}_{i+2}), \tag{26}$$

$$\hat{f}^{-}_{i+1/2} = \Xi(f^{-}_{i+3}, f^{-}_{i+2}, f^{-}_{i+1}, f^{-}_{i}, f^{-}_{i-1}), \tag{27}$$

and

$$f^{+}_{i} = \frac{1}{2}(f(\mathbf{u}_i) + \alpha \mathbf{u}_i), \tag{28}$$

$$f^{-}_{i} = \frac{1}{2}(f(\mathbf{u}_i) - \alpha \mathbf{u}_i), \tag{29}$$

where

$$\alpha = \max(|f'(\mathbf{u}_i)|, |f'(\mathbf{u}_{i+1})|). \tag{30}$$

Following Ref. 6, the interpolating function $\Xi(a, b, c, d, e)$ is defined next. First, define three interpolated values:

$$q_1 = \frac{a}{3} - \frac{7b}{6} + \frac{11c}{6}, \tag{31}$$

$$q_2 = -\frac{b}{6} + \frac{5c}{6} + \frac{d}{3}, \tag{32}$$

$$q_3 = \frac{c}{3} + \frac{5d}{6} - \frac{e}{6}, \tag{33}$$

and three indicators of smoothness, β:

$$\beta_1 = 13(a - 2b + c)^2 + 3(a - 4b + 3c)^2, \tag{34}$$

$$\beta_2 = 13(b - 2c + d)^2 + 3(d - b)^2, \tag{35}$$

$$\beta_3 = 13(c - 2d + e)^2 + 3(3c - 4d + e)^2, \tag{36}$$

then take

$$\alpha_1 = \frac{1}{(\epsilon + \beta_1)^2}, \tag{37}$$

$$\alpha_2 = \frac{6}{(\epsilon + \beta_2)^2}, \tag{38}$$

$$\alpha_3 = \frac{3}{(\epsilon + \beta_3)^2}, \tag{39}$$

and define the weights[29]

$$w_i = \frac{\alpha_i}{\alpha_1 + \alpha_2 + \alpha_3}. \tag{40}$$

It was noted[6] that these weights could be significantly improved to yield a more robust method that truly converged at fifth order with a new set of $\bar{\alpha}_i$ defined by

$$\bar{\alpha}_1 = \frac{w_1(11 - 30w_1 + 100w_1^2)}{1 + 80w_1} \tag{41}$$

$$\bar{\alpha}_2 = \frac{w_2(24 - 45w_2 + 25w_2^2)}{9 - 5w_2} \tag{42}$$

$$\bar{\alpha}_3 = \frac{w_3(39 - 90w_3 + 100w_3^2)}{9 + 40w_3} \tag{43}$$

to yield

$$\Xi(a, b, c, d, e) = \frac{\bar{\alpha}_1 q_1 + \bar{\alpha}_2 q_2 + \bar{\alpha}_3 q_3}{\bar{\alpha}_1 + \bar{\alpha}_2 + \bar{\alpha}_3}. \tag{44}$$

In all computations presented here, $\epsilon = 10^{-40}$, as suggested in Ref. 6.

3. Nodes $N_x - 2 \leq i \leq N_x - 1$

The discretization at node i needs information at the nodes $i-3, ..., i+3$. Since differencing across the shock at $x = 0$ is ill-advised, something else will need to be done for the nodes $i = N_x - 2$, $i = N_x - 1$ and $i = N_x$. At these nodes, an explicit formula is taken for the components of the flux derivatives, which is biased in such a manner that no nodes $i > N_x$ are used. These are derived from standard Taylor series expansions (TSE). In particular, the numerical approximation to each component of the flux is given by

$$\frac{\partial}{\partial x}\left(f\left(\mathbf{u}_{N_x-2}\right)\right) \approx \frac{-2f\left(\mathbf{u}_{N_x-5}\right) + 15f\left(\mathbf{u}_{N_x-4}\right) - 60f\left(\mathbf{u}_{N_x-3}\right) + 20f\left(\mathbf{u}_{N_x-2}\right) + 30f\left(\mathbf{u}_{N_x-1}\right) - 3f\left(\mathbf{u}_{N_x}\right)}{60\Delta x}, \tag{45}$$

and

$$\frac{\partial}{\partial x}\left(f\left(\mathbf{u}_{N_x-1}\right)\right) \approx \frac{-f\left(\mathbf{u}_{N_x-4}\right) + 6f\left(\mathbf{u}_{N_x-3}\right) - 18f\left(\mathbf{u}_{N_x-2}\right) + 10f\left(\mathbf{u}_{N_x-1}\right) + 3f\left(\mathbf{u}_{N_x}\right)}{12\Delta x}. \tag{46}$$

Equation (45), according to TSE, is fifth order accurate. Also, it can be shown that Eq. (46) is, by TSE, only fourth order accurate. This lower order scheme, at this single point, seemed to be necessary for linear numerical stability. It is seen later that this did not induce any noticeable degradation in the solution. This point is not along a characteristic, and so fourth order errors do not have a chance to accumulate at this point in the flow. The source term, $\mathbf{s}\left(\mathbf{u}_i\right)$, is still just an evaluation at these two nodes.

4. Node $i = N_x$

At the shock locus, $i = N_x$, the solution is only a function of the shock velocity, D. At this point, only Eq. (19) is solved. Only the momentum flux gradient needs to be computed to update the shock velocity. Here, a biased fifth order stencil,

$$\frac{\partial}{\partial x}\left(f\left(\mathbf{u}_{N_x}\right)\right) \approx \frac{-12f\left(\mathbf{u}_{N_x-5}\right) + 75f\left(\mathbf{u}_{N_x-4}\right) - 200f\left(\mathbf{u}_{N_x-3}\right) + 300f\left(\mathbf{u}_{N_x-2}\right) - 300f\left(\mathbf{u}_{N_x-1}\right) + 137f\left(\mathbf{u}_{N_x}\right)}{60\Delta x}, \tag{47}$$

is used to calculate the momentum flux gradient.

The conservative state variables at the shock are given from the shock jump relations, Eqs. (6-9). No source terms enter at this nodal point, since this is exactly a shock state. Also, the numerical method is discretely conservative everywhere, except at $i = N_x$, since the state there is constrained to be at a shock state, and so itself cannot be discretely conservative. Errors in conservation are of the order of the truncation error of the scheme, and so are small.

C. Temporal Discretization

With the discrete operator $\mathbf{L}$ now defined, Eqs. (22) could be solved by a wide variety of standard numerical techniques, explicit or implicit, which have been developed over the years for large systems of ordinary differential equations. Here, an explicit six-stage Runge-Kutta scheme[7] with fifth order temporal accuracy is chosen.

Most Runge-Kutta schemes of fourth or higher order are easier to code and seem to require less storage when the Butcher formulation[7,28] is chosen rather than the more commonplace $\alpha-\beta$ form.[5] Given a solution $\mathbf{u}_i^n$ at t_n, the solution $\mathbf{u}_i^{n+1}$ at t_{n+1} is constructed in the following manner. The generic s-stage Butcher formulation of Runge-Kutta schemes takes on the form

$$\bar{\mathbf{u}}_i^1 = \mathbf{u}_i^n, \tag{48}$$

$$\bar{\mathbf{u}}_i^j = \mathbf{u}_i^n + \Delta t_n \sum_{k=1}^{j-1} a_{jk} \mathbf{L}\left(\bar{\mathbf{u}}_i^k\right), \qquad j = 2, ..., s, \tag{49}$$

where $\bar{\mathbf{u}}_i^j$ are the intermediate solution states at each j-stage, and the solution at the next time step is given by

$$\mathbf{u}_i^{n+1} = \mathbf{u}_i^n + \Delta t_n \sum_{j=1}^{s} b_j \mathbf{L}\left(\bar{\mathbf{u}}_i^j\right). \tag{50}$$

The coefficients, a_{jk} and b_j in the above formulæ are given in Tables 1 and 2, respectively.

	$k=1$	$k=2$	$k=3$	$k=4$	$k=5$
$j=2$	1				
$j=3$	$\frac{1}{4}$	$\frac{1}{4}$			
$j=4$	$\frac{2046}{15625}$	$-\frac{454}{15625}$	$\frac{1533}{15625}$		
$j=5$	$-\frac{739}{5625}$	$\frac{511}{5625}$	$-\frac{566}{16875}$	$\frac{20}{27}$	
$j=6$	$\frac{11822}{21875}$	$-\frac{6928}{21875}$	$-\frac{4269}{21875}$	$-\frac{4}{7}$	$\frac{54}{35}$

Table 1. Runge-Kutta coefficients a_{jk}.

$b_1 = \frac{1}{24}$
$b_2 = 0$
$b_3 = 0$
$b_4 = \frac{125}{336}$
$b_5 = \frac{27}{56}$
$b_6 = \frac{5}{48}$

Table 2. Runge-Kutta coefficients b_j.

In this problem, for which the effect of the source term has been resolved, it is convection which dictates the time step restriction. All computations performed here have $0.8 < CFL < 1.5$, where CFL represents the traditional Courant-Friedrichs-Lewy number. The high order of the Runge-Kutta method enables CFL to be slightly greater than unity while maintaining numerical stability. The results were verified to be insensitive to small changes in CFL.

IV. Results

Results are given for a set of standard test cases. All calculations were performed on a four-processor Compaq ES45 workstation with a clock speed of 1 GHz and 64-bit arithmetic. The typical computation

time for any single case was ten minutes. A few calculations which required long integration times took many hours to complete. The equations have been scaled in such a fashion that the ambient density and pressure are $\rho_o = 1$ and $p_o = 1$, the half-reaction zone length, $L_{1/2}$, is unity, and other parameters take the values $q = 50$, and $\gamma = 1.2$. Here $L_{1/2}$ is the distance from the shock to the point at which λ takes on the value $1/2$ for the steady ZND structure. This now standard approach requires one to vary k from case to case in order to maintain $L_{1/2} = 1$; for $E = 25$, one has $k = 35.955584760859722$, where the high precision is needed to guarantee the high precision of the results.

Here, interest is focused on self-sustained detonation waves, known commonly as Chapman-Jouguet (CJ).[25] This results in a steady detonation velocity of

$$D_{CJ} = \sqrt{11} + \sqrt{\frac{61}{5}} \approx 6.80947463. \tag{51}$$

Interest is further focused on how increase in the activation energy, E, affects the propagation of the detonation wave. Linear stability analysis[10] reveals that for $E < 25.26$, the steady ZND detonation wave structure[25] will be linearly stable, and for $E > 25.26$, the steady detonation structure is linearly unstable. In all cases considered, the exact, to machine precision, ZND solution is used as the initial condition. Note that using 64-bit machine precision translates to roughly 16 significant figures. A second comparison case is presented in the following subsection for $E = 26$.

In all unstable cases considered, the predicted non-linear behavior has its origin in a single unstable low frequency mode identified by linear theory. While evermore high frequency modes are predicted by the linear theory as E increases through a series of threshold values, here, E is increased only moderately. As a consequence, the high frequency instabilities are suppressed, while still admitting a rich spectrum of low frequency non-linear behavior.

A. Linearly Stable ZND, $E = 25$

The new algorithm is first tested on a stable problem, $E = 25$, and results are compared with those of a recent shock-fitting study.[19] For this case, the steady solution is stable, and thus it is the exact solution for all time. This can also serve as a test problem for verification of the numerical scheme. As done in Ref. 19, the numerically calculated detonation velocity can be plotted as a function of time. In particular, it is important to measure the error produced as a function of numerical resolution. Following Ref. 19, one defines the number of numerical zones in the half reaction zone length to be $N_{1/2}$, so that $\Delta x = 1/N_{1/2}$. Figure 1 shows the result of Kasimov and Stewart's numerical method for $N_{1/2} = 100$ and $N_{1/2} = 200$. At relatively long times, this numerical method attains $D_{N_{1/2}=100} \approx 6.8285$ and $D_{N_{1/2}=200} \approx 6.8189$. Considering the numerical errors, ΔD, are then 0.0190 and 0.0094, respectively, it is concluded that the error of the scheme of Ref. 19 scales directly with Δx, and is thus first order accurate. These results are summarized in Table 3 below, where r_c is the rate of convergence.

$N_{1/2}$	ΔD	r_c
100	1.90×10^{-2}	-
200	9.40×10^{-3}	1.01

Table 3. Numerical accuracy of Ref. 19.

The prediction of the high order shock-fitting algorithm of the previous section, utilizing a coarser grid, $N_{1/2} = 20$, is displayed in Fig. 2. A few important facts should be noted. First, the error in shock speed has been greatly reduced by the high order shock-fitting scheme, even utilizing a much coarser grid. This is evident because of greatly reduced scale on the detonation velocity in Fig. 2. Also, not only are the errors greatly reduced, but the rate of convergence is predicted to be fifth order. This can be seen in Table 4. Thus, for this stable problem, the new high order shock-fitting scheme produces very accurate solutions with moderate mesh size.

B. Linearly Unstable ZND, Stable Limit Cycle, $E = 26$

Next, an unstable problem, $E = 26$, is analyzed, as also done in Ref. 19. For $E = 26$, linear stability theory[15] predicts a single unstable mode, with growth rate, $\sigma_r = 0.03710$, and a frequency, $\sigma_i = 0.52215$. Figure 3

$N_{1/2}$	ΔD	r_c
20	2.13×10^{-6}	-
40	6.00×10^{-8}	5.01

Table 4. Numerical accuracy of high order shock-fitting scheme.

gives a plot of the numerical prediction of detonation velocity, D, as a function of time, with $N_{1/2} = 20$. The growth of the unstable mode is triggered by the small numerical truncation error. Figure 3 shows a clearly oscillatory exponential growth of $D(t)$ at early times ($t < 300$). Postulating that the numerical predictions could be fit by an equation of the form

$$D(t) \sim a_0 + a_1 e^{a_2 t} \sin(a_3 t + a_4), \tag{52}$$

a least squares curve fit of the data over the range $0 < t < 100$ revealed that

$$a_0 = 6.80947239809145 \pm 7.506 \times 10^{-10}, \tag{53}$$
$$a_1 = 0.00000643598884 \pm 4.549 \times 10^{-10}, \tag{54}$$
$$a_2 = 0.03709980167992 \pm 7.983 \times 10^{-7}, \tag{55}$$
$$a_3 = 0.52214295442142 \pm 8.615 \times 10^{-7}, \tag{56}$$
$$a_4 = 0.18145671900944 \pm 7.455 \times 10^{-5}. \tag{57}$$

Note that the growth rate a_2 and wavenumber a_3 both agree strikingly to five significant figures with the predictions of linear stability theory.

Note from Fig. 3 that the long time behavior appears to be that of a stable periodic limit cycle. One can thus infer that the non-linear effects are stabilizing the linear instability, and that the amplitude of the long time limit cycle is dictated by a balance struck between linear growth and non-linear decay. It is useful to plot the results in the phase plane, dD/dt versus D.[13] This is easily and accurately accomplished, since the shock acceleration, dD/dt, is already computed from the shock-change equation (19). Figure 4 is the parametric plot of dD/dt versus D, where both the acceleration and velocity are known parametrically as functions of t. The solution starts at $dD/dt(t = 0) = 0$, and $D(t = 0) = D_{CJ}$. A spiral trajectory commences at this point and has a radius of curvature which increases with arc length which is indicative of the linear instability. At late times, $t > 350$, the solution has effectively relaxed to a steady cyclic behavior. It is also noted that through several numerical simulations, the linear stability boundary was determined to be located at $E = 25.265 \pm 0.005$, in excellent agreement with the prediction of linear stability theory.

C. Period-Doubling and Feigenbaum's Universal Constant

As noted in Ref. 17, and later in Ref. 20, if the activation energy is increased to $E \approx 27.2$, one predicts a period-doubling phenomena, reminiscent of that predicted by the simple logistic map.[30,31] Figure 5 shows the time history of the detonation velocity for the case $E = 27.35$. It is evident that in the long time limit the solution possesses two distinct relative maxima, namely $D \approx 8.225$ and $D \approx 7.676$; whereas for $E = 26$, only a single relative maximum, $D \approx 7.439$ is predicted. The corresponding phase plane is shown in Fig. 6. Performing several simulations, with $N_{1/2} = 20$, to long times (up to $t = 30000$), one can bisect the region $26 < E < 27.35$, in an attempt to find the bifurcation point, *i.e.* the point where the single periodic cycle gives way to the period-2 solution. The activation energy at this point will be denoted by E_1. Likewise, as noted in Ref. 20, there are other period-doubling bifurcation values of E_n, where the solution transits from a period-2^{n-1} to a period-2^n. The point at which one predicts the transition from a steady solution (linear stability) to a periodic solution (period-1 solution) will be designated by E_0. These bifurcation points, and their numerical uncertainty are given in Table 5. Also calculated are the differences between these points, $E_{n+1} - E_n$, and the relative change in the differences, δ_n:

$$\delta_n = \frac{E_n - E_{n-1}}{E_{n+1} - E_n}. \tag{58}$$

It was predicted by Feigenbaum,[26,27] using models of several different physical and mathematical phenomena, that in the limit as $n \to \infty$, that δ_n approaches a universal constant, $\delta_\infty \approx 4.669201$, now commonly known as Feigenbaum's number. Table 5 shows three progressively better approximations, δ_1, δ_2, and δ_3, to δ_∞. It is seen that δ_3 is in agreement with δ_∞, with an uncertainty of 2%.

n	E_n	$E_{n+1} - E_i$	δ_n
0	25.265 ± 0.005	-	-
1	27.1875 ± 0.0025	1.9225 ± 0.0075	3.86 ± 0.05
2	27.6850 ± 0.001	0.4975 ± 0.0325	4.26 ± 0.08
3	27.8017 ± 0.0002	0.1167 ± 0.0012	4.66 ± 0.09
4	27.82675 ± 0.00005	0.02505 ± 0.00025	-

Table 5. Numerically determined bifurcation points and approximations to Feigenbaum's number.

D. Bifurcation Diagram, Semi-Periodic Solutions, Odd Periods, Windows and Chaos

Given that the solutions obtained, even for $N_{1/2} = 10$, are so accurate and efficient to calculate, a detailed bifurcation diagram can be constructed with much greater detail than any to date. It is noted that Ref. 20 did show the first bifurcation diagram for this model, albeit with only twenty-five different activation energies. Here, the bifurcation diagram is constructed by sampling over a thousand different activation energies, with $25 < E < 28.4$ with $\Delta E = 0.0025$. At each value of E, the exact ZND solution is used as the initial condition. For each E, the solution is integrated to $t = 5000$, and all the relative maxima in D are recorded for $3000 < t < 5000$ (*i.e.* the late time behavior). This composite plot of predicted, late time, relative maxima in D versus E is presented in Fig. 7. The qualitative similarities to the logistic map are striking. One clearly notices the various period-doubling bifurcations up to roughly $E_\infty \approx 27.8324$. One then notes various regions of semi-periodic behavior, and various odd-periodic regions. For example in the vicinity of $E = 28.2$, a large period-3 window opens in the bifurcation diagram; as E is increased further, the period-3 solution bifurcates. In regions where the bifurcation points are very dense, it is likely that the system has underwent a transition to chaos.

Figure 8 gives several plots of D versus t as activation energy is increased. Specific values of E are listed in the caption. In Fig. 8a), a period-4 solution is shown. As E is increased, the system continues a bifurcation process, and a chaotic state is realized in general. However, in b), c), and d) examples are found which are within windows of order in an otherwise chaotic region. Periods of 6, 5, and 3 are found, respectively. In e), a chaotic solution is shown. In f) another structured solution is found with period-3.

Note that as the system becomes more chaotic, the solution remains resolved. This is because the periods are increasing, not decreasing. However, for much higher activation energies, roughly $E > 30$, higher frequency instabilities are excited, and finer resolution would be necessary. Moreover, at such high activation energies, secondary shocks may form, which would negate the advantage of the present shock-fitting method.

V. Discussion

The results for the simple model problem suggest that when properly employed, algorithm craftsmanship in the form of shock-fitting coupled with a high order spatio-temporal discretization can yield remarkable gains in accuracy of many orders of magnitude relative to existing algorithms for certain specialized problems. This then admits solution in more rapid fashion or enables existing computational resources to be used to predict new phenomena. While advances in hardware have certainly increased computational predictive capabilities, it must be admitted that, even accounting for the unlikely unfettered continuation of Moore's Law, *realization of the algorithm-driven accuracy gains achieved here by reliance instead on hardware improvements alone would require several years, if not decades, to achieve.* One can in fact consider the method presented here to be the algorithmic analog to either the Hubble telescope or an electron microscope: *a tool which strikingly slashes the error amplitude so as to bring into tight focus fine scale features orders of magnitude beyond previous capability.*

Certainly, the specifications of the particular problem considered here facilitated these improvements. Comparable gains for more general problems would require careful effort or may be impossible to achieve. For

inviscid problems with multiple embedded discontinuities, the shock-fitting procedure becomes intractable, for example. For problems with diffusion, high order methods are easier to employ, but at the expense of having to address problems with a wide variety of length scales, which taxes computational hardware and software in a different way. Certainly also, customized algorithm design is initially more time-consuming relative to off-the-shelf production codes. But, if one seeks an accurate solution of equations which simulate key paradigm physical problems, investment in algorithm development can often prove to be a dramatically more effective use of resources than investment in hardware.

Acknowledgments

This study was performed under the auspices of the U. S. Department of Energy. The authors thank A. R. Kasimov and D. S. Stewart for sharing their numerical solutions for various cases presented in this paper. They also thank G. J. Sharpe and M. Short for providing detailed growth rates and frequencies used in comparisons, and H. D. Ng for useful discussions regarding the path to instability.

References

[1] Moore, G. E., "Cramming More Components onto Integrated Circuits," *Electronics*, Vol. 38, No. 8, 1965, pp. 114-117.

[2] Lundstrom, M., "Moore's Law Forever?," *Science*, Vol. 299, No. 5604, 2003, pp. 210-211.

[3] Yungster, S., and Radhakrishnan, K., "Pulsating One-Dimensional Detonations in Hydrogen-Air Mixtures," *Combustion Theory and Modelling*, Vol. 8, No. 4, 2004, pp. 745-770.

[4] Powers, J. M., and Paolucci, S., "Accurate Spatial Resolution Estimates for Reactive Supersonic Flow with Detailed Chemistry," *AIAA Journal*, to appear; also, AIAA Paper 2005-1171.

[5] Shu, C.-W., and Osher, S., "Efficient Implementation of Essentially Non-Oscillatory Schemes for Hyperbolic Conservation Laws," *Journal of Computational Physics*, Vol. 77, No. 2, 1988, pp. 439-471.

[6] Henrick, A. K., Aslam, T. D., and Powers, J. M., "Mapped Weighted Essentially Non-Oscillatory Schemes: Achieving Optimal Order Near Critical Points," *Journal of Computational Physics*, in review.

[7] Macdonald, C. B., "Constructing High-Order Runge-Kutta Methods with Embedded Strong-Stability-Preserving Pairs," M. Sc. Thesis, Simon Fraser University, August 2003.

[8] Erpenbeck, J. J., "Stability of Steady-State Equilibrium Detonations," *Physics of Fluids*, Vol. 5, No. 5, 1962, pp. 604-614.

[9] Fickett, W., and Wood, W. W.,"Flow Calculations for Pulsating One-Dimensional Detonations," *Physics of Fluids*, Vol. 9, 1966, pp. 903-916.

[10] Lee, H. I., and Stewart, D. S., "Calculation of Linear Detonation Instability: One-Dimensional Instability of Plane Detonation," *Journal of Fluid Mechanics*, Vol. 216, 1990, pp. 103-132.

[11] Bourlioux, A., Majda, A. J., and Roytburd, V., "Theoretical and Numerical Structure for Unstable One-Dimensional Detonations," *SIAM Journal on Applied Mathematics*, Vol. 51, No. 2, 1991, pp. 303-343.

[12] He, L., and Lee, J. H. S., "The Dynamical Limit of One-Dimensional Detonations," *Physics of Fluids*, Vol. 7, No. 5, 1995, pp. 1151-1158.

[13] Yao, J., and Stewart, D. S., "On the Dynamics of Multi-Dimensional Detonation," *Journal of Fluid Mechanics*, Vol. 309, 1996, pp. 225-275.

[14] Short, M., "Multidimensional Liner Stability of a Detonation Wave at High Activation Energy," *SIAM Journal of Applied Mathematics*, Vol. 57, No. 2, 1997, pp. 307-326.

[15] Sharpe, G. J., "Linear Stability of Idealized Detonations," *Proceedings of the Royal Society A*, Vol. 453, No. 1967, 1997, pp. 2603-2625.

[16] Hwang, P., Fedkiw, R. P., Merriman, B., Aslam, T. D., Karagozian, A. R., and Osher, S. J. "Numerical resolution of pulsating detonation waves," *Combustion Theory and Modelling*, Vol. 4, No. 3, 2000, pp. 217-240.

[17] Sharpe, G. J., and Falle, S. A. E. G., "Numerical Simulations of Pulsating Detonations: I. Nonlinear Stability of Steady Detonations," *Combustion Theory and Modelling*, Vol. 4, No. 4, 2000, pp. 557-574.

[18] Aslam, T. D., "A Level Set Algorithm for Tracking Discontinuities in Hyperbolic Conservation Laws II: Systems of Equations," *Journal of Scientific Computing*, Vol. 19, Nos. 1-3, 2003, pp. 37-62.

[19] Kasimov, A. R., and Stewart, D. S., "On the Dynamics of Self-Sustained One-Dimensional Detonations: a Numerical Study in the Shock-Attached Frame," *Physics of Fluids*, Vol. 16, No. 10, 2004, pp. 3566-3578.

[20] Ng, H. D., Higgins, A. J., Kiyanda, C. B., Radulescu, M. I., Lee, J. H. S., Bates, K. R., and Nikiforakis, N. "Nonlinear Dynamics and Chaos Analysis of One-Dimensional Pulsating Detonations," *Combustion Theory and Modelling*. (in press), 2005.

[21] Majda, A., and Osher, S., "Propagation of Error into Regions of Smoothness for Accurate Difference Approximations to Hyperbolic Equations," *Communications on Pure and Applied Mathematics*, Vol. 30, No. 6, 1977, pp. 671-705.

[22] Casper, J., and Carpenter, M. H., "Computational Consideration for the Simulation of Shock-Induced Sound," *SIAM Journal on Scientific Computing*, Vol. 19, No. 3, 1998, pp. 818-828.

[23] Carpenter, M. H., and Casper, J. H., "Accuracy of Shock Capturing in Two Spatial Dimensions," *AIAA Journal*, Vol. 37, No. 9, 1999, pp. 1072-1079.

[24] Powers, J. M., and Aslam, T. D., "Exact Solutions for Two-Dimensional Reactive Flow for Verification of Numerical Algorithms," AIAA Paper 2005-1173, Jan. 2005 (submitted to the *AIAA Journal*).

[25] Fickett, W., and Davis, W., *Detonation*, University of California Press, Berkeley, CA, 1979.

[26] Feigenbaum, M. J., "Quantitative Universality for a Class of Non-Linear Transformations," *Journal of Statistical Physics*, Vol. 19, No. 1, 1978, pp. 25-52.

[27] Feigenbaum, M. J., "The Universal Metric Properties of Nonlinear Transformations," *Journal of Statistical Physics*, Vol. 21, No. 6, 1979, pp. 669-706.

[28] Burden, R. L., and Faires, J. D., *Numerical Analysis*, Prindle, Weber and Schmidt, Boston, MA, 1985.

[29] Jiang, G.-S. and Shu, C.-W., "Efficient Implementation of Weighted ENO Schemes," *Journal of Computational Physics*, Vol. 126, No. 1, 1996, pp. 202-228.

[30] Jackson, E. A., *Perspectives on Nonlinear Dynamics*, Cambridge University Press, New York, NY, 1991.

[31] Drazin, P. G., *Nonlinear Systems*, Cambridge University Press, New York, NY, 1992.

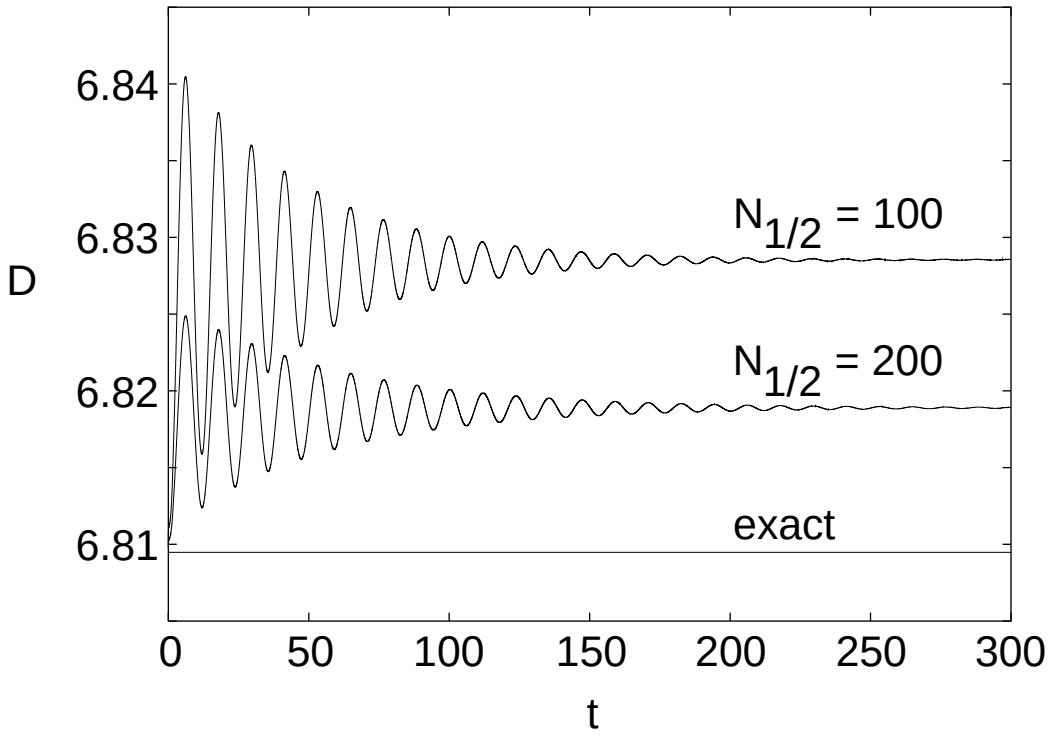

Figure 1. Numerically generated detonation velocity, D versus t, using the shock-fitting scheme of Kasimov and Stewart,[19] $E = 25$, $q = 50$, $\gamma = 1.2$, with $N_{1/2} = 100$ and $N_{1/2} = 200$.

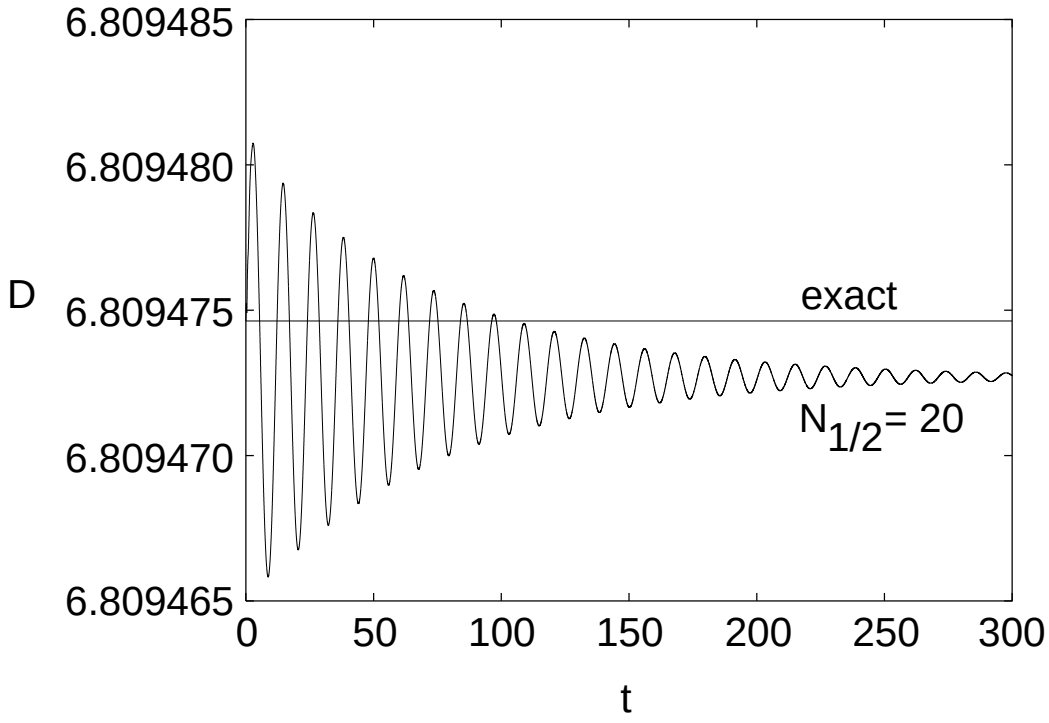

Figure 2. Numerically generated detonation velocity, D versus t, using the high order shock-fitting scheme, $E = 25$, $q = 50$, $\gamma = 1.2$, with $N_{1/2} = 20$.

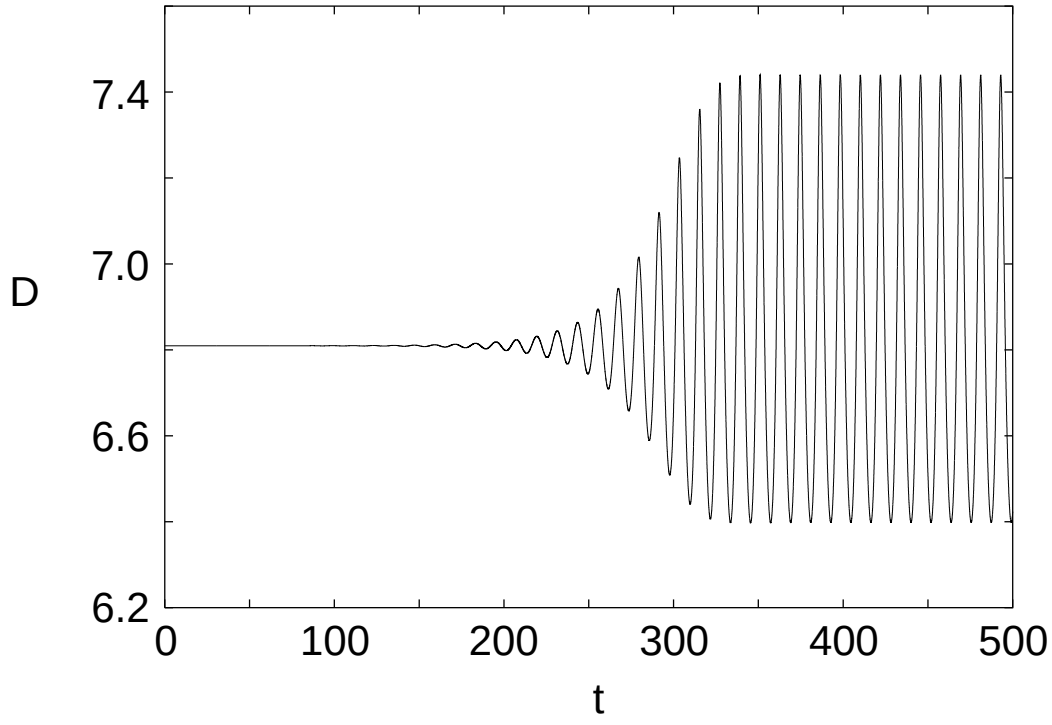

Figure 3. Numerically generated detonation velocity, D versus t, using the high order shock-fitting scheme, $E = 26$, $q = 50$, $\gamma = 1.2$, with $N_{1/2} = 20$. Period-1 oscillations shown.

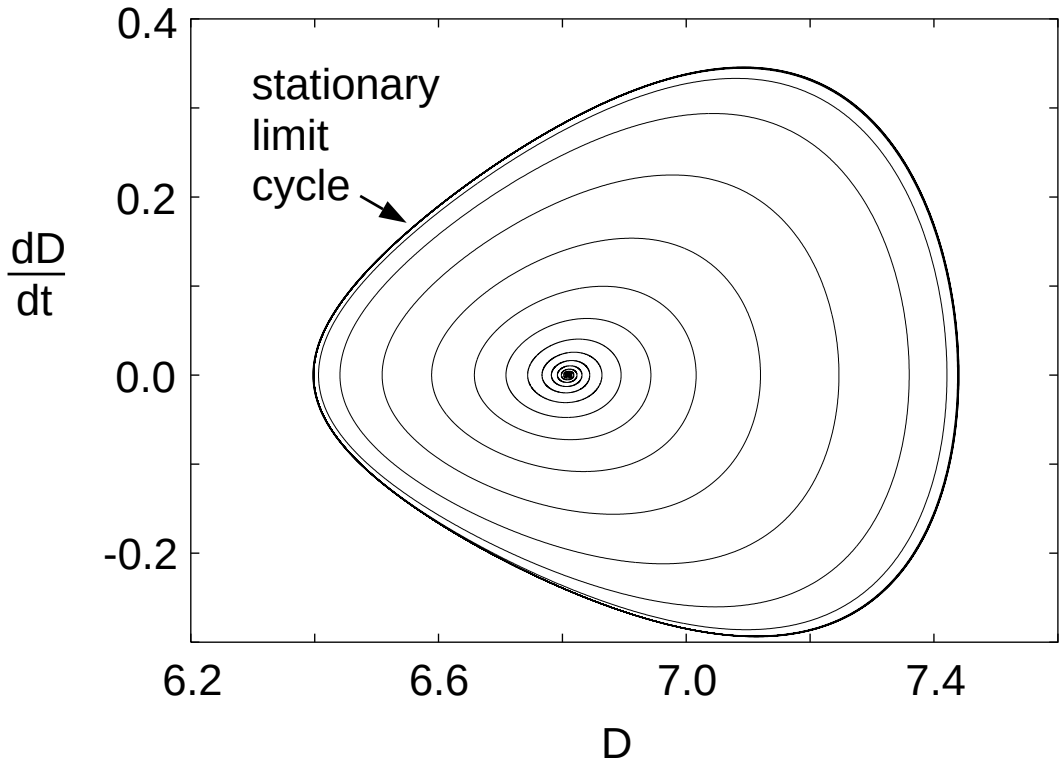

Figure 4. Numerically generated phase portrait dD/dt versus D, using the high order shock-fitting scheme, $E = 26$, $q = 50$, $\gamma = 1.2$, with $N_{1/2} = 20$. Period-1 oscillations shown.

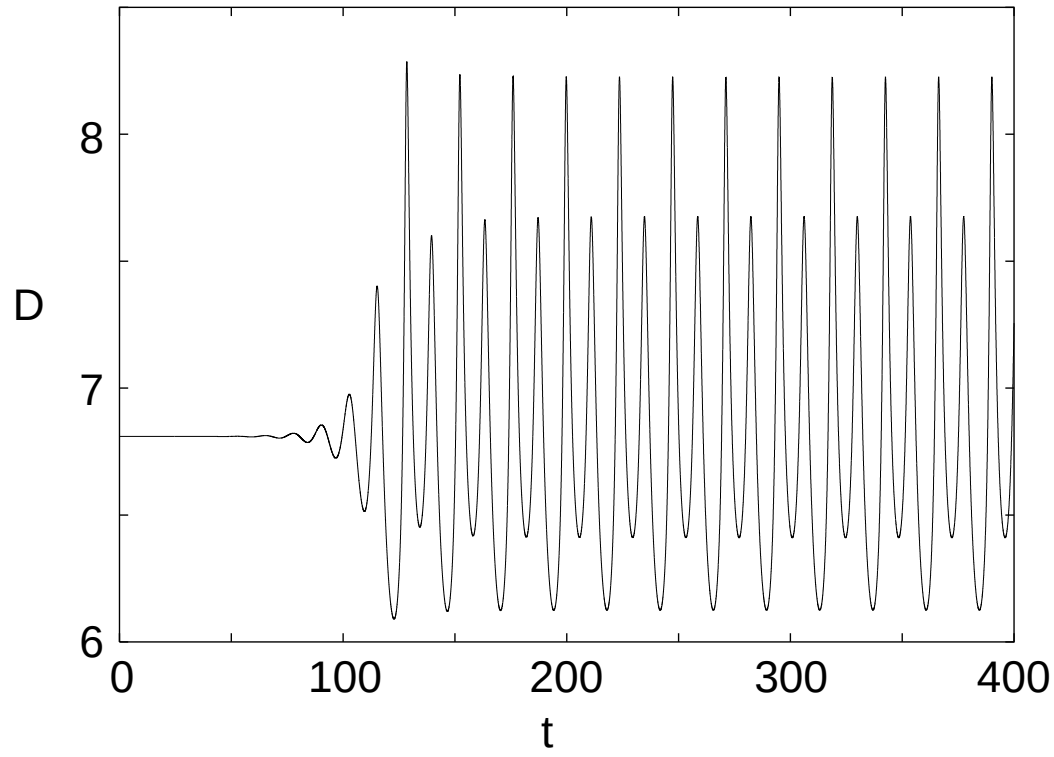

Figure 5. Numerically generated detonation velocity, D versus t, using the high order shock-fitting scheme, $E = 27.35$, $q = 50$, $\gamma = 1.2$, with $N_{1/2} = 20$. Period-2 oscillations shown.

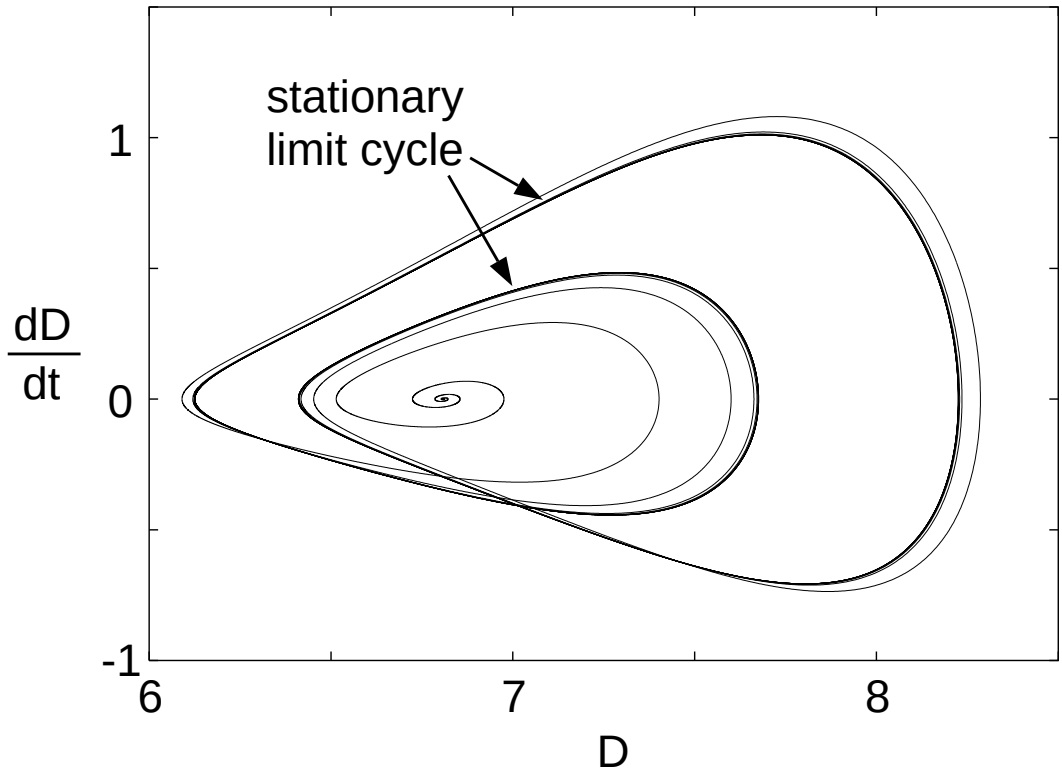

Figure 6. Numerically generated phase portrait dD/dt versus D using the high order shock-fitting scheme, $E = 26$, $q = 50$, $\gamma = 1.2$, with $N_{1/2} = 20$. Period-2 oscillations shown.

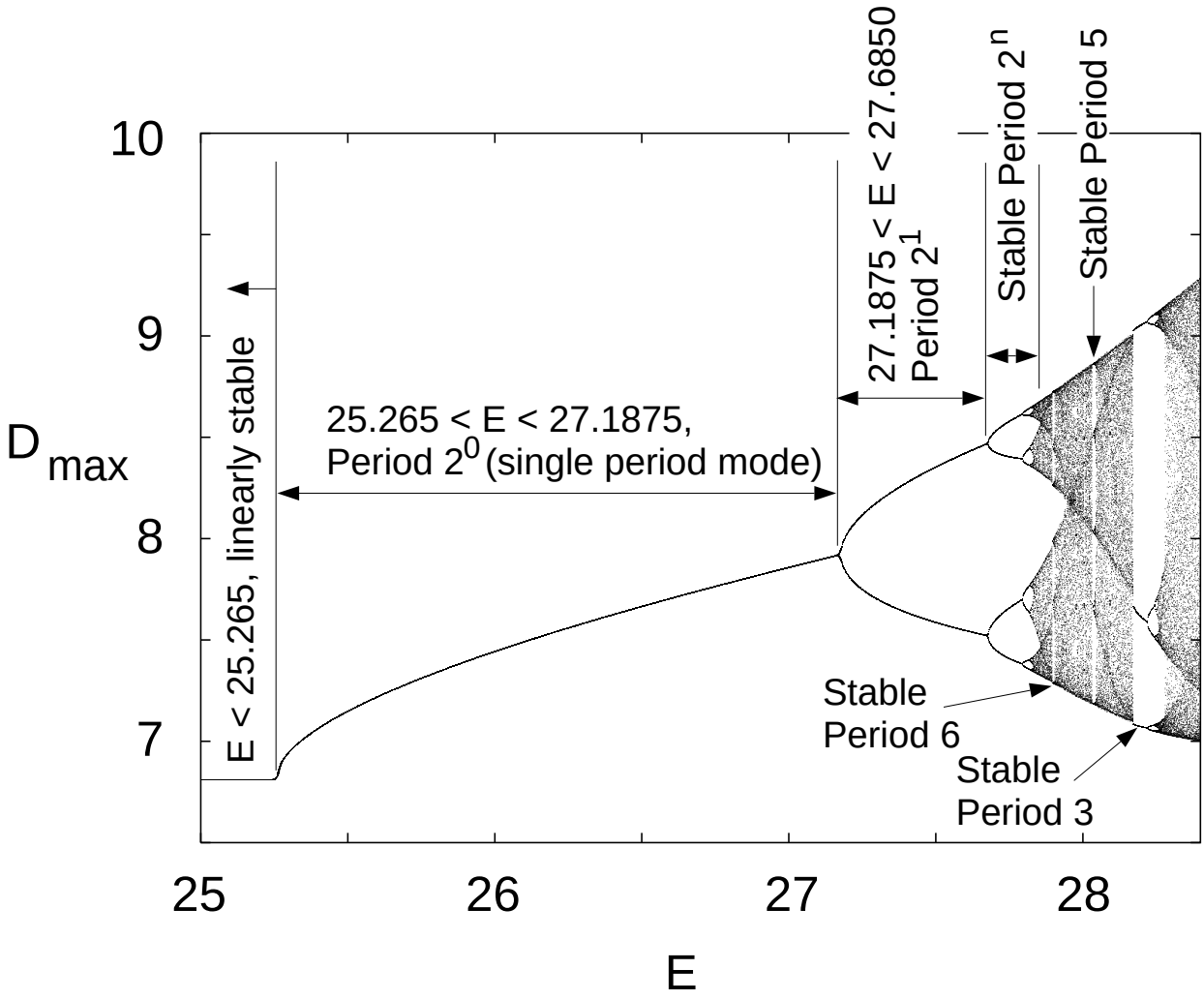

Figure 7. Numerically generated bifurcation diagram, $25 < E < 28.4$**,** $q = 50$**,** $\gamma = 1.2$**.**

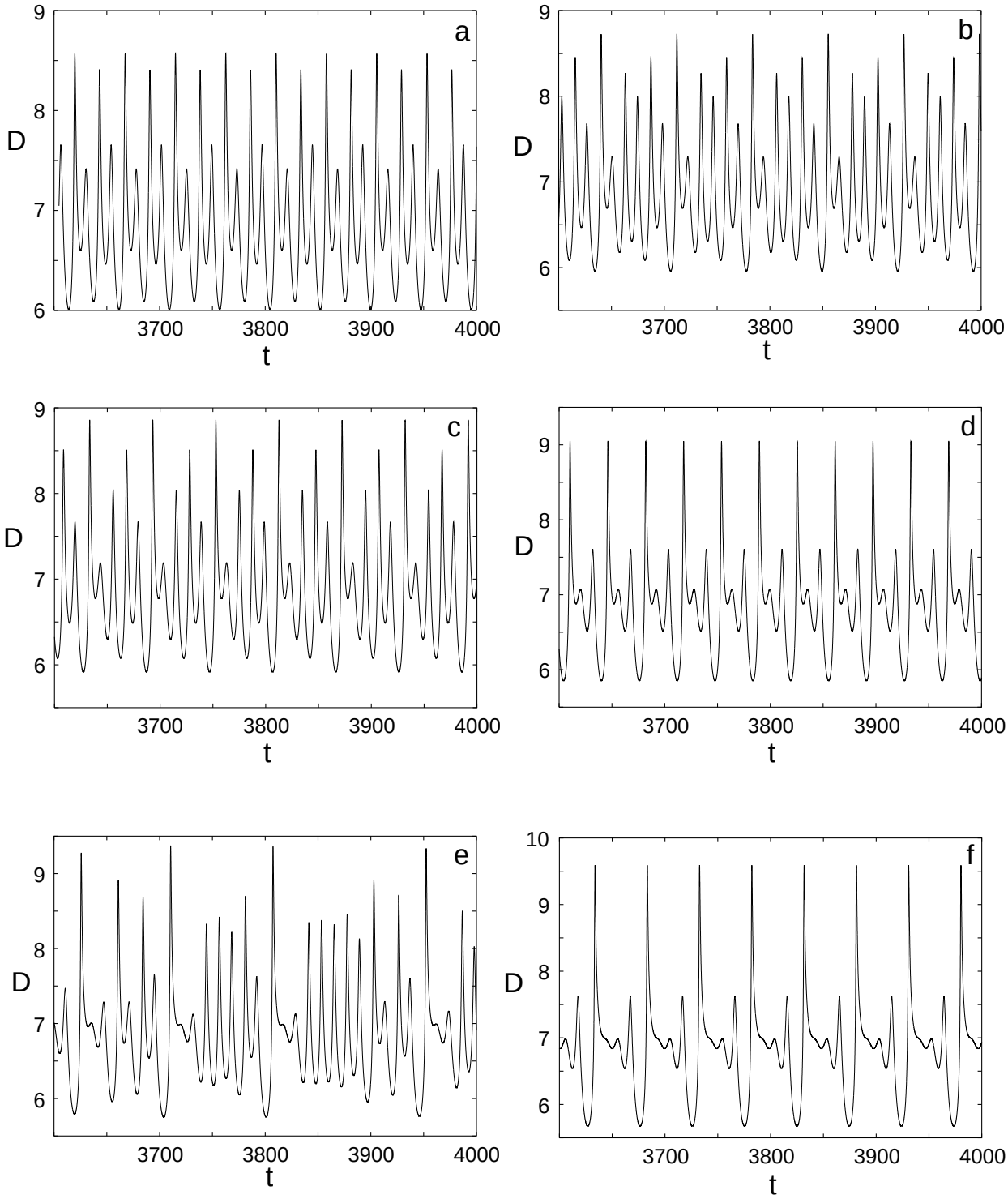

Figure 8. Numerically generated detonation velocity, D versus t, using the high order shock-fitting scheme, $q = 50$, $\gamma = 1.2$, with $N_{1/2} = 20$, a) $E = 27.75$, period-4, b) $E = 27.902$, period-6, c) $E = 28.035$, period-5, d) $E = 28.2$, period-3, e) $E = 28.5$, chaotic, f) $E = 28.66$, period-3.